

Thermally activated double-carrier transport in epitaxial graphene on vanadium-compensated 6H-SiC as revealed by Hall effect measurements

Tymoteusz Ciuk^{a,*}, Andrzej Kozłowski^a, Paweł Piotr Michałowski^a,
Wawrzyniec Kaszub^a, Michał Kozubal^{a,b}, Zbigniew Rekuc^a, Jarosław Podgórski^a,
Beata Stanczyk^a, Krystyna Przyborowska^a, Iwona Jozwik^a, Andrzej Kowalik^a,
Paweł Kamiński^a

^a Institute of Electronic Materials Technology, Wolczynska 133, 01-919, Warsaw, Poland

^b VIGO System S.A., Poznańska 129/133, 05-850, Warsaw, Poland

ARTICLE INFO

Article history:

Received 23 April 2018

Received in revised form

18 July 2018

Accepted 22 July 2018

Available online 23 July 2018

Keywords:

Graphene

Epitaxy

CVD

Hall effect

Sensor

Atomic layer deposition

Transport properties

ABSTRACT

In this report we demonstrate the results of charge carriers transport studies in graphene using a Hall effect sensor fabricated on quasi-free-standing monolayer graphene grown on a semi-insulating on-axis vanadium-compensated 6H-SiC(0001) substrate in an epitaxial Chemical Vapor Deposition process. The sensor is passivated with aluminum oxide through atomic layer deposition and offers current-mode sensitivity of 140 V/AT with thermal stability of $-0.02\%/K$ within the range between 80 and 573 K. The electrical properties of the graphene layer are determined as a function of temperature ranging from 300 to 770 K. High-temperature characteristics of passivated and not passivated graphene are compared and their profiles explained through a *double-carrier* transport involving the spontaneous-polarization-induced holes in the graphene layer and the thermally activated electrons from a shallow donor level of nitrogen in the quasi-cubic (k_T) site and a deep acceptor level of vanadium in the hexagonal (h) site both present in the bulk of the vanadium-compensated SiC substrate. Finally, we conclude that this mechanism is directly responsible for the limitation of the thermal stability of the sensor's current-mode sensitivity.

© 2018 Elsevier Ltd. All rights reserved.

1. Introduction

The Hall effect sensors widely found in industrial applications, including brushless direct current electric motors (BLDC), permanent magnet synchronous motors (PMSM) and electric current sensors for power usage monitoring are typically realized in CMOS, GaAs, InAs or InSb technologies. Being semiconducting in nature, these materials offer an interplay between linearity, thermal stability and sensitivity. Depending on whether these sensors are current driven or voltage driven their sensitivity is defined as either current-mode $S_I = (\frac{\partial U_{Hall}}{\partial B})/I = 1/p_s e$ [V/AT] or voltage-mode $S_V = (\frac{\partial U_{Hall}}{\partial B})/V = \mu W/L$ [V/VT], where U_{Hall} is the Hall voltage, B is the magnetic field, I is the driving current, p_s is the sheet charge carrier

concentration, e is the unit charge, V is the driving voltage, μ is the carrier mobility and W/L are the dimensions of the active layer. The gain in current-mode sensitivity of $S_I^{GaAs} \sim 160$ V/AT, $S_I^{InAs} \sim 330$ V/AT and $S_I^{InSb} \sim 2000$ V/AT [1] is at the cost of ever reduced thermal stability as the semiconductor's energy bandgap narrows from $E_g^{GaAs} \sim 1.424$ eV, through $E_g^{InAs} \sim 0.354$ eV, to $E_g^{InSb} \sim 0.17$ eV at 300 K. Their temperature range of application is typically limited to (233 K, 398 K). A state-of-the-art low-current CMOS technology offers the operating free-air temperature range of (218 K, 473 K) [2]. In Ref. [3] the authors report on a n -InSb/GaAs Hall effect sensor with a thermally stable $S_I \sim 3$ V/AT in the range between 3 K and 573 K.

In recent years, several groups reported on application of graphene in the technology of a Hall effect sensor, emphasizing the significance of the current-mode sensitivity and the magnetic field resolution. These works include graphene grown on copper foil and transferred onto a SiO₂/n-Si substrate [4], monolayer graphene epitaxially grown on SiC [5], graphene grown on platinum and

* Corresponding author.

E-mail address: tymoteusz.ciuk@itme.edu.pl (T. Ciuk).

transferred onto a SiO₂/Si substrate [6], one-two layer epitaxial sublimated graphene grown on 4H-SiC(0001) [7], and mechanically exfoliated graphene encapsulated in hexagonal boron nitride (hBN) [8]. In the previous paper we have shown a complete Hall effect sensor [9] made from quasi-free-standing (QFS) monolayer graphene grown on semi-insulating (SI) vanadium-compensated 6H-SiC(0001) substrate in an epitaxial Chemical Vapor Deposition (CVD) process. That sensor was passivated with a silicone encapsulant to ensure its electrical stability and environmental resistance and its current-mode sensitivity of 87 V/AT was defined at room temperature.

In this work, we not only present an advanced Hall effect sensor that is based on QFS-monolayer graphene grown in an industrial epitaxial CVD technology but also define its current-mode sensitivity in a wide range of temperatures between 80 and 770 K. From the sensor's characteristics we draw original scientific conclusions on charge carrier transport in graphene on silicon carbide and verify its applicability in high-temperature magnetic field detection.

2. Experimental details

2.1. Graphene epitaxy and the Hall effect sensor technology

The sensor has the form of a *van der Pauw* structure, 2 mm in width and length, and utilizes the classical Hall effect to produce Hall voltage. The sensor's active area is made from QFS-monolayer graphene obtained through hydrogen atom intercalation of a sole buffer layer grown on a SI vanadium-compensated on-axis 15 × 15 mm² 6H-SiC(0001) substrate (II-VI Inc.) using the epitaxial CVD method [10] in a standard hot-wall CVD Aixtron VP508 reactor.

The device processing cycle has been developed on the Vistec SB251 electron-beam lithography system. The Hall sensor features an equal-arm cross-shaped active area terminated with Ti/Au (10 nm/60 nm) ohmic contacts. Fig. 1a illustrates 21 sensors on the 10 × 10 mm² working area of the 15 × 15 mm² 6H-SiC(0001) substrate. A single 2 × 2 mm² Hall structure is depicted in Fig. 1b and its scanning electron microscope image in Fig. 1c.

2.2. Aluminum oxide passivation

In Ref. [9] we described the application of a silicone as an encapsulant for graphene and verified its suitability for the Hall effect sensor operation at room temperature. In this report, we introduce an aluminum oxide passivation realized in a high-temperature atomic layer deposition process in the 4-in Picosun R200 Advanced reactor. The aluminum oxide layer is deposited from trimethylaluminum (TMA, Al₂(CH₃)₆) and deionized water at 770 K. Residual carbon content, originating from an incomplete reaction between TMA and water, was chosen as an indicator of the deposition quality and monitored with Secondary Ion Mass Spectrometry (SIMS), since the method is particularly useful for the ALD quality assessment [11]. A CAMECA SC Ultra instrument operating under ultra-high vacuum (typically 4 × 10⁻¹⁰ mbar) was applied. High dynamic range was reached with the impact energy of 13 keV for Cs⁺ primary ions and the negative ions detection mode. The intensity of the primary beam was set at the level of 50 nA. The beam swept the area of 300 × 300 μm², and the analysis was limited to 200 × 200 μm². No mass interference was expected for ¹²C⁻ ions, thus a mass resolving power $m/\Delta m = 400$ was used throughout the experiment. Fig. 2 illustrates the carbon profile in a 40-nm-thick aluminum oxide layer deposited on a test silicon substrate at 770 K. The interface is marked with a peak in the carbon content. The SIMS analysis proves that the synthesis is optimum and that the carbon levels in the oxide and in the commercial silicon substrate are in a comparable range.

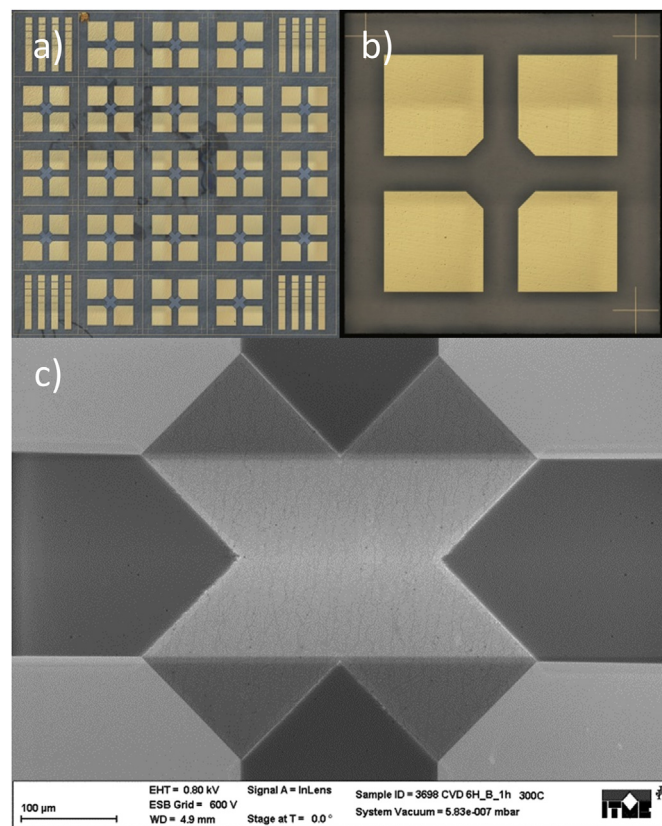


Fig. 1. a) Optical image of 21 Hall effect sensors made from QFS hydrogen-intercalated monolayer graphene grown in an epitaxial CVD process on a SI vanadium-compensated on-axis 15 × 15 mm² 6H-SiC(0001) substrate. b) Optical image of a single 2 × 2 mm² Hall structure. c) Scanning electron microscope image of the Hall sensor's active area in the form of an equal-arm cross (the horizontal, dark and light pattern is an effect induced by the difference in conductivity among selected parts of an ungrounded specimen). (A colour version of this figure can be viewed online.)

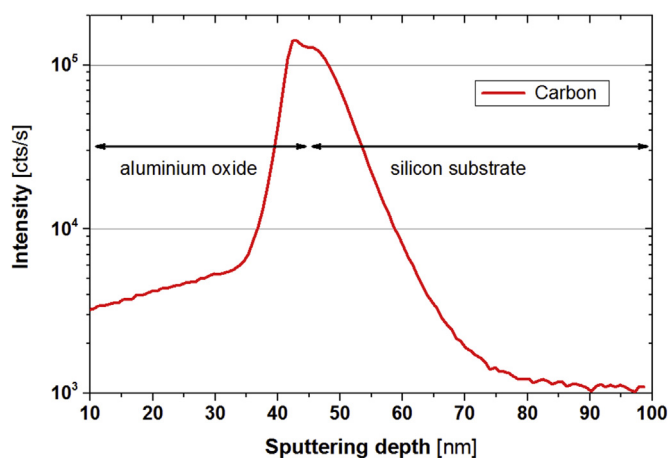


Fig. 2. Residual carbon profile in a 40-nm-thick aluminum oxide layer synthesized at 770 K from trimethylaluminum (TMA) and H₂O on a test silicon substrate in the Picosun R200 Advanced atomic layer deposition reactor. (A colour version of this figure can be viewed online.)

For the purpose of an in-depth analysis of charge carrier transport in epitaxial graphene on SiC out of the 21 sensors depicted in Fig. 1 (a) four were chosen. For reasons explained in the next sections the first sensor was left not passivated, one was

passivated with a 40-nm-thick aluminum oxide layer described above, one with a 100-nm-thick aluminum oxide layer under the same process conditions, and one had the graphene layer fully removed with an oxygen plasma, so that bare 6H-SiC(0001) remained between the ohmic contacts.

In order to facilitate the measurement the $2 \times 2 \text{ mm}^2$ sensors were mounted and bonded to a custom-made $10 \times 10 \text{ mm}^2$ sapphire holder equipped with four Cr/Au (100 nm/20 nm) corner contacts, so that the Hall setup probes could be placed onto the holder pads.

2.3. Electrical characterization

The sensors were fed with $I = 1 \text{ mA}$ direct current and the sheet charge carrier concentration p_s [cm^{-2}], mobility μ_p [cm^2/Vs], sheet resistance R_S [Ω/sq] and current-mode sensitivity $S_I = (\frac{\partial U_{Hall}}{\partial B})/I = 1/p_s e$ [V/AT], where e is the unit charge, were characterized with the use of an Ecopia automated Hall effect measurement system equipped with a neodymium 0.556 T magnet (a low-temperature AMP55 unit in the range between 80 and 300 K and a high-temperature AHT55T5 unit in the range between 300 and 770 K).

The environmental resistance of the passivation was verified in the Hall effect sensor passivated with a 100-nm-thick aluminum oxide layer. This sensor was fed with $I = 1 \text{ mA}$ and characterized in a static magnetic field of 0.556 T at temperatures between 80 and 770 K. The other two sensors, one passivated with a 40-nm-thick aluminum oxide layer and one without passivation were measured in the high-temperature range only.

3. Experimental results and discussion

3.1. Hall effect sensor characteristics

At room temperature (300 K) the sensor passivated with the 100-nm-thick aluminum oxide layer offers $S_I \sim 136 \text{ V/AT}$, which is higher than previously reported for the silicone-encapsulated Hall effect sensor [9]. At 80 K the sensor is characterized by $S_I \sim 141 \text{ V/AT}$. The current-mode sensitivity is greatly stable up to 573 K, where $S_I \sim 127 \text{ V/AT}$, and only at higher temperatures S_I decreases, eventually reaching $S_I \sim 65 \text{ V/AT}$ at 770 K (red line in Fig. 3).

In the range between 80 K and 573 K, the thermal stability defined as $\frac{(S_I^2 - S_I^1)}{S_I^1(T_2 - T_1)} \times 100\%$, where $T_1 = 80 \text{ K}$ and $T_2 = 573 \text{ K}$, is negative and equals $-0.02\%/K$, which is a remarkable achievement given the wide range of temperatures ($\Delta T = 493 \text{ K}$). In order to prove the sensor's resistance to the changing environmental conditions, the device was subject to an aging test in a ZUT Michalin climatic chamber. During 17 h the temperature rose from 300 K to 343 K, then fell to 243 K, and back to 300 K, while humidity varied between 0% at the lowest temperatures and 100% at the highest. After the test the sensor was stored for 6 weeks in ambient conditions. The repeated current-mode sensitivity profile (blue line in Fig. 3) almost matches the primary one (an average increase of 2% in the range between 80 K and 573 K was observed) and confirms the good quality of the aluminum oxide passivation. What is also important for application no degradation of the Ti/Au contacts was observed. However, the profile of the current-mode sensitivity curve and its steep decline above 573 K requires further detailed explanation.

3.2. Transport properties as a function of temperature

In order to explain the current-mode sensitivity profile, the three sensors (one without passivation, one passivated with a 40-nm-thick aluminum oxide layer, and one passivated with a 100-nm-thick aluminum oxide layer) were characterized in a static

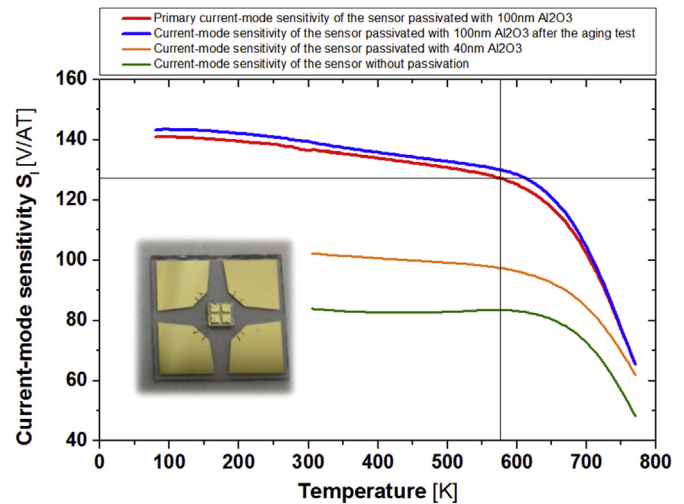


Fig. 3. Temperature profile of the current-mode sensitivity S_I of the Hall effect sensors made from QFS hydrogen-intercalated monolayer graphene grown in an epitaxial CVD process on a Si vanadium-compensated on-axis 6H-SiC(0001) substrate and passivated with an aluminum oxide layer deposited at 770 K from TMA and water precursors. The characteristics of three graphene sensors (not passivated, passivated with a 40-nm-thick aluminum oxide layer and passivated with a 100-nm-thick aluminum oxide layer) are compared. In the case of the sensor covered with a 100-nm-thick passivation the red line represents the primary profile and the blue line is the repeated profile after the aging test and 6-week storing in ambient conditions. (A colour version of this figure can be viewed online.)

magnetic field of 0.556 T at temperatures between 300 and 770 K. The fourth one, with the graphene layer fully removed with an oxygen plasma, was characterized in a narrower range between 420 and 770 K.

As expected, graphene conductance measured in the not passivated sensor is of p -type and the hole concentration is consistent with the theoretically predicted $p_s^{6H} \approx 7.5 \times 10^{12} \text{ cm}^{-2}$ for *as-grown* QFS epitaxial graphene on 6H-SiC(0001) [12–14], as governed by the vector of the spontaneous polarization of 6H-SiC [15–17].

It remains unaffected by the temperature up to approx. 620 K, at which point a steep rise begins. Qualitatively, similar curvature is observed in the sensor passivated with a 40-nm-thick aluminum oxide layer (orange line in Fig. 4a) and with a 100-nm-thick passivation (red line in Fig. 4a), although the dielectric screening effect of the oxide suppresses the influence of the excess surface bound charge of SiC (spontaneous polarization) and pins the room-temperature hole concentration at $p_s \approx 6.1 \times 10^{12} \text{ cm}^{-2}$ (for 40-nm aluminum oxide layer) and $p_s \approx 4.6 \times 10^{12} \text{ cm}^{-2}$ (100-nm aluminum oxide layer). The experimentally observed relative thermal stability of p_s below approx. 620 K results from the constant value of the spontaneous polarization of 6H-SiC in the range between 0 meV and approx. 120 meV ($\sim 1400 \text{ K}$) as theoretically calculated by Slawinska et al. [17]. However, its rise at elevated temperatures above approx. 620 K requires further explanation.

The fourth Hall sensor that had the graphene layer fully removed in an oxygen plasma, so that only bare 6H-SiC(0001) surface remained between the ohmic contacts was fed with direct current $I = 1 \text{ mA}$ and characterized in the automated Hall measurement system in accordance with the procedure adapted for the not passivated and the passivated graphene layers. At room temperature, as expected, the resistivity of Si 6H-SiC substrate proved very high. However, starting from approx. 473 K, an exponentially growing sheet concentration of hardly mobile electrons (black line in Fig. 4a) appeared, suggesting thermal activation of defect levels in the bulk of the SiC crystal according to the exponent of the

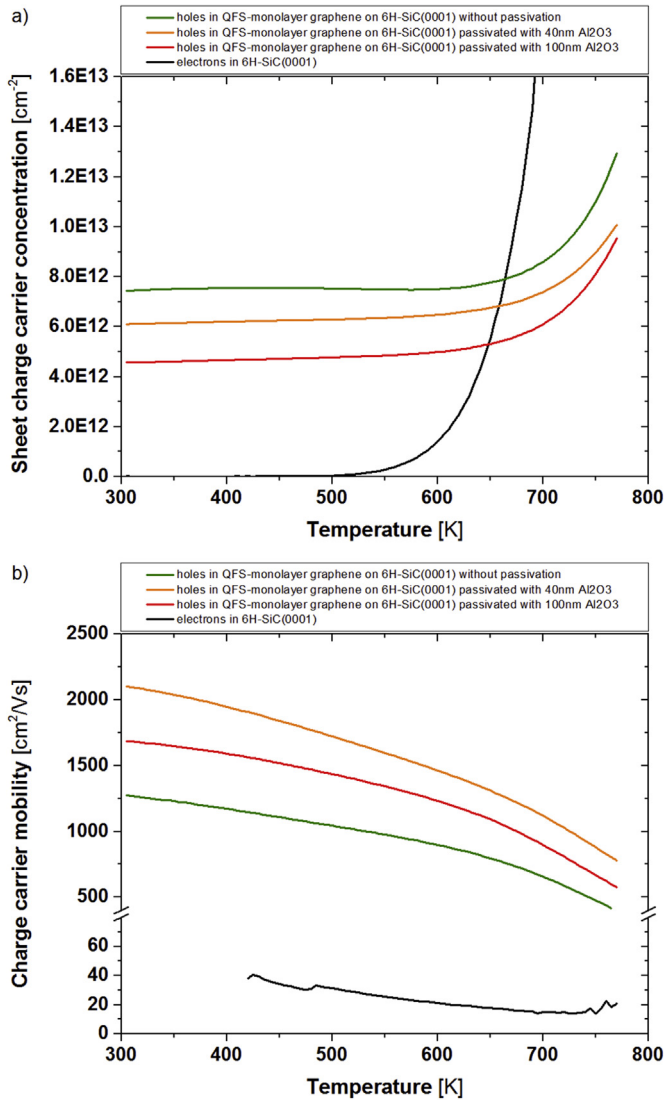


Fig. 4. As-measured sheet charge carrier concentration (a) and mobility (b) as a function of temperature in the range between 300 and 770 K measured by means of a Hall effect sensor made from QFS hydrogen-intercalated monolayer graphene grown in an epitaxial CVD process on a Si vanadium-compensated on-axis 6H-SiC(0001) substrate. The characteristics of three graphene layers (not passivated, passivated with a 40-nm-thick aluminum oxide layer and passivated with a 100-nm-thick aluminum oxide layer) as well as of a Si 6H-SiC(0001) surface layer made by fully removing the graphene layer in an oxygen plasma, are compared. (A colour version of this figure can be viewed online.)

Arrhenius equation $\exp(-E_a/k_B T)$, where E_a is the activation energy, k_B is the Boltzmann constant and T is the absolute temperature. Converted to a natural logarithm as a function of the inverse of $k_B T$, the curve (black line in Fig. 5) revealed two activation energies, $E_a \approx 100$ meV at lower temperatures and $E_a \approx 905$ meV at higher temperatures. We attribute these energies to a shallow donor level of nitrogen in the quasi-cubic (k_1) site and to a deep acceptor level of vanadium in the hexagonal (h) site, respectively. These levels were identified by High-Resolution Photoinduced Transient Spectroscopy (HRPITS) [18,19].

The experimentally observed thermal activation of the shallow and the deep defect levels in the bulk of the vanadium-compensated SiC substrate suggests that the high-temperature transport in epitaxial quasi-free-standing graphene is governed by two types of charge carriers, namely the spontaneous-polarization-induced holes in graphene ($p_{s(gr)}$, $\mu_{p(gr)}$) and the

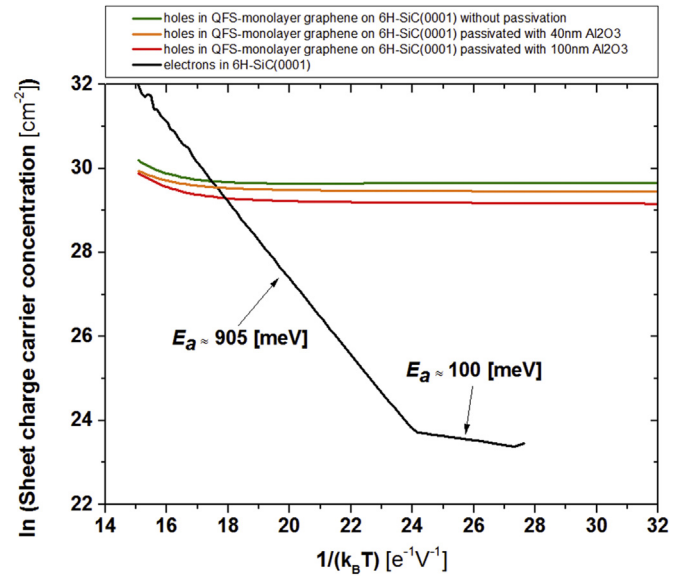


Fig. 5. Natural logarithm of as-measured sheet charge carrier concentration as a function of the inverse of $k_B T$ in the range between 300 K and 770 K measured in a Hall effect made from QFS hydrogen-intercalated monolayer graphene grown in an epitaxial CVD process on a Si vanadium-compensated on-axis 6H-SiC(0001) substrate. The characteristics of three graphene layers (not passivated, passivated with a 40-nm-thick aluminum oxide layer and passivated with a 100-nm-thick aluminum oxide layer) as well as of a Si 6H-SiC(0001) surface layer made by fully removing the graphene layer in an oxygen plasma, are compared. (A colour version of this figure can be viewed online.)

thermally activated electrons in silicon carbide ($n_{s(SiC)}$, $\mu_{n(SiC)}$). Therefore, it should be referred to as *double-carrier* instead of *single-carrier* as anticipated by the Hall measurement system.

In the *single-carrier* model the Hall coefficient is defined as $R_H = 1/p_s e$ and the sheet resistance as $R_S^{-1} = e p_s \mu_p$, where e is the unit charge, p_s is the sheet hole concentration, and μ_p is the hole

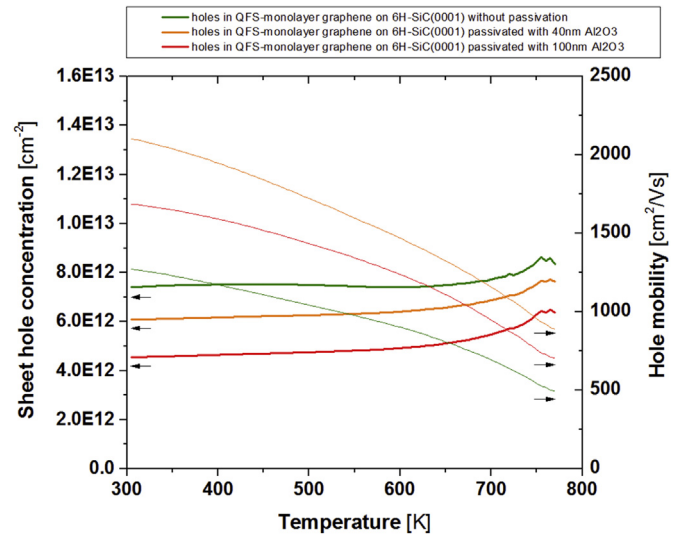


Fig. 6. Extracted hole concentration and mobility as a function of temperature in the range between 300 and 770 K measured by means of a Hall effect sensor made from QFS hydrogen-intercalated monolayer graphene grown in an epitaxial CVD process on a Si vanadium-compensated on-axis 6H-SiC(0001) substrate. The results for a not passivated graphene layer, one passivated with a 40-nm-thick aluminum oxide layer and one passivated with a 100-nm-thick aluminum oxide layer are compared. (A colour version of this figure can be viewed online.)

Table 1
Summary of the current-mode sensitivity S_I , measured hole concentration p_s and mobility μ_p in QFS hydrogen-intercalated monolayer graphene grown in an epitaxial CVD process on a Si vanadium-compensated on-axis 6H-SiC(0001) substrate, measured electron concentration $n_{s(\text{SiC})}$ and mobility $\mu_{n(\text{SiC})}$ in the bare Si vanadium-compensated on-axis 6H-SiC(0001) substrate and the extracted hole concentration $p_{s(\text{gr})}$ and mobility $\mu_{p(\text{gr})}$ in the bare graphene layer, experimentally observed in a not passivated and aluminum-oxide-passivated Hall effect sensors at 300 K, 600 K and 700 K.

Aluminum oxide passivation	Current-mode sensitivity S_I [V/AT]	p_s [cm ⁻²]	μ_p [cm ² /Vs]	$p_{s(\text{gr})}$ [cm ⁻²]	$\mu_{p(\text{gr})}$ [cm ² /Vs]
Temperature 300 K					
$n_{s(\text{SiC})} = 2.2 \times 10^{10}$ cm ⁻² , $\mu_{n(\text{SiC})} = 46$ cm ² /Vs					
No passivation	84	7.4×10^{12}	1273	7.4×10^{12}	1273
40 nm	102	6.1×10^{12}	2103	6.1×10^{12}	2103
100 nm	136	4.6×10^{12}	1686	4.6×10^{12}	1686
Temperature 600 K					
$n_{s(\text{SiC})} = 1.4 \times 10^{12}$ cm ⁻² , $\mu_{n(\text{SiC})} = 21$ cm ² /Vs					
No passivation	83	7.5×10^{12}	898	7.4×10^{12}	902
40 nm	96	6.5×10^{12}	1463	6.4×10^{12}	1468
100 nm	125	5.0×10^{12}	1232	4.9×10^{12}	1238
Temperature 700 K					
$n_{s(\text{SiC})} = 1.9 \times 10^{13}$ cm ⁻² , $\mu_{n(\text{SiC})} = 15$ cm ² /Vs					
No passivation	73	8.6×10^{12}	658	7.7×10^{12}	693
40 nm	85	7.4×10^{12}	1119	6.9×10^{12}	1158
100 nm	102	6.1×10^{12}	899	5.5×10^{12}	947

mobility. Instead, a *double-carrier* model should be introduced where $R_H = \frac{p_{s(\text{gr})}\mu_{p(\text{gr})}^2 - n_{s(\text{SiC})}\mu_{n(\text{SiC})}^2}{e(p_{s(\text{gr})}\mu_{p(\text{gr})} + n_{s(\text{SiC})}\mu_{n(\text{SiC})})^2}$, and $R_S^{-1} = e(p_{s(\text{gr})}\mu_{p(\text{gr})} + n_{s(\text{SiC})}\mu_{n(\text{SiC})})$. Assuming the *double-carrier* model and based on the experimental temperature profile of $n_{s(\text{SiC})}$ and $\mu_{n(\text{SiC})}$ (black lines in Fig. 4) and R_S for either the not passivated or the passivated graphene layers, one can solve for the product of $p_{s(\text{gr})}\mu_{p(\text{gr})}$. In the second step, knowing $n_{s(\text{SiC})}$, $\mu_{n(\text{SiC})}$, $p_{s(\text{gr})}\mu_{p(\text{gr})}$ and R_H measured for the not passivated and the passivated graphene layers, one can separately draw the $p_{s(\text{gr})}$ and $\mu_{p(\text{gr})}$ curves.

It becomes evident from the *extracted* profiles of the hole concentration $p_{s(\text{gr})}$ and mobility $\mu_{p(\text{gr})}$ in graphene (Fig. 6) that it is the *measured* hole concentration p_s (Fig. 4a) that is in particular affected by the build-up of electrons in the substrate. Since the current-mode sensitivity of a Hall effect sensor is inversely proportional to the *measured* hole concentration p_s , the observed thermal activation of the shallow and the deep defect states in the bulk of the SiC substrate is directly responsible for the limitation of the substantial thermal stability of S_I . A summary of the experimental data is presented in Table 1.

One may expect that if the vanadium-compensated 6H-SiC substrate in which the high resistivity is achieved mainly through the compensation of boron acceptors ($E_a \approx 280$ meV and $E_a \approx 430$ meV) with deep vanadium donors ($E_a \approx 1320$ meV and $E_a \approx 1405$ meV) located at various lattice sites [19] was replaced with high-purity undoped 6H-SiC the effect of the thermal activation of vanadium-related levels would no longer affect the Hall effect sensor properties. However, even the high-purity undoped 6H-SiC contains traps related to residual impurities (E_a ranging from 80 meV to 1900 meV) occupying the hexagonal h and the two quasi-cubic sites k_1 and k_2 . The mechanism responsible for its semi-insulating properties is complex and involves residual nitrogen donors and boron acceptors, residual vanadium donors and acceptors, as well as deep-level native defects which atomic configuration remains unknown [18]. Therefore, it is advisable that the high-temperature transport properties of QFS graphene on SiC remain a subject of further scientific study.

4. Conclusions

In this report we have shown an advanced Hall effect sensor in the form of an equal-arm, fully symmetrical *van der Pauw* structure made from QFS hydrogen-intercalated monolayer graphene grown in an epitaxial CVD process on a Si vanadium-compensated on-axis

6H-SiC(0001) substrate. The atomic-layer-deposited passivation of the graphene layer was performed at 770 K from trimethylaluminum (TMA) and H₂O.

We have proven that the Hall effect sensor with a graphene layer passivated with a 100-nm-thick aluminum oxide layer is environmentally resistant, offers the current-mode sensitivity of 140 V/AT with thermal stability of $-0.02\%/K$ within the range between 80 and 573 K, and is applicable to high-temperature magnetic field detection.

Finally, upon analysis of the graphene layer electrical properties in a wide range of temperatures between 300 and 770 K, we have demonstrated the presence of a *double-carrier* transport that involves the spontaneous-polarization-induced holes in the graphene layer and the thermally activated electrons from the defect levels related to nitrogen donors and vanadium acceptors in the bulk of the Si 6H-SiC substrate. We conclude that this mechanism is directly responsible for the limitation of the thermal stability of the current-mode sensitivity.

Acknowledgements

The authors would like to cordially thank Wlodek Strupinski, PhD, for providing epitaxial graphene on silicon carbide samples.

The research leading to these results has received funding from the National Centre for Research and Development under Grant Agreement No. LIDER 0168/L-8/2016 for project “*Graphene on silicon carbide devices for magnetic field detection in extreme temperature conditions*” and under Grant Agreement No. TECHMAT-STRATEG1/346922/4/NCBR/2017 for project “*Technologies of semiconductor materials for high power and high frequency electronics*”. This work has been also partially supported by the European Union's Horizon 2020 research and innovation programme under grant agreement No. 785219.

Appendix A. Supplementary data

Supplementary data related to this article can be found at <https://doi.org/10.1016/j.carbon.2018.07.049>.

References

- [1] Asahi Kasei Microdevices Corporation, www.akm.com.
- [2] Micropac Industries, Inc., www.micropac.com.
- [3] J. Jankowski, S. El-Ahmar, M. Oszwaldowski, Hall sensors for extreme temperatures, *Sensors* 11 (2011) 876–885.

- [4] C.C. Tang, M.Y. Li, L.J. Li, C.C. Chi, J.C. Chen, Characteristics of a sensitive micro-Hall probe fabricated on chemical vapor deposited graphene over the temperature range from liquid-helium to room temperature, *Appl. Phys. Lett.* 99 (2011) 112107.
- [5] V. Panchal, K. Cedergren, R. Yakimova, A. Tzalenchuk, S. Kubatkin, O. Kazakova, Small epitaxial graphene devices for magnetosensing applications, *J. Appl. Phys.* 111 (2012), 07E509.
- [6] H. Xu, L. Huang, Zh Zhang, B. Chen, H. Zhong, L.M. Peng, Flicker noise and magnetic resolution of graphene hall sensors at low frequency, *Appl. Phys. Lett.* 103 (2013) 112405.
- [7] R.K. Rajkumar, A. Asenjo, V. Panchal, A. Manzin, O. Iglesias-Freire, O. Kazakova, Magnetic scanning gate microscopy of graphene Hall devices, *J. Appl. Phys.* 115 (2014) 172606.
- [8] J. Dauber, A.A. Sagade, M. Oellers, K. Watanabe, T. Taniguchi, D. Neumaier, Ch Stampfer, Ultra-sensitive Hall sensors based on graphene encapsulated in hexagonal boron nitride, *Appl. Phys. Lett.* 106 (2015) 193501.
- [9] T. Ciuk, O. Petruk, A. Kowalik, I. Jozwik, A. Rychter, J. Szmidi, W. Strupinski, „Low-noise epitaxial graphene on SiC Hall effect sensor for commercial applications, *Appl. Phys. Lett.* 108 (2016) 223504.
- [10] W. Strupinski, K. Grodecki, A. Wysmolek, R. Stepniowski, T. Szkopek, P.E. Gaskell, Graphene epitaxy by chemical vapor deposition on SiC, *Nano Lett.* 11 (4) (2011) 1786–1791.
- [11] P.P. Michalowski, V. Beyer, M. Czernohorsky, P. Kucher, S. Teichert, G. Jaschke, W. Moller, Formation of an interface layer between $Al_{1-x}Si_xO_y$ thin films and the Si substrate during rapid thermal annealing, *Phys. Status Solidi C* 7 (2010) 284–287.
- [12] T. Ciuk, S. Cakmakyapan, E. Ozbay, P. Caban, K. Grodecki, A. Krajewska, I. Pasternak, J. Szmidi, W. Strupinski, „Step-edge-induced resistance anisotropy in quasi-free-standing bilayer chemical vapor deposition graphene on SiC, *J. Appl. Phys.* 116 (2014) 123708.
- [13] T. Ciuk, W. Strupinski, Statistics of epitaxial graphene for Hall effect sensors, *Carbon* 93 (2015) 1042–1049.
- [14] T. Ciuk, P. Caban, W. Strupinski, Charge Carrier concentration and offset voltage in quasi-free-standing monolayer chemical vapor deposition graphene on SiC, *Carbon* 101 (2016) 431–438.
- [15] J. Ristein, S. Mammadov, Th Seyller, Origin of doping in quasi-free-standing graphene on silicon carbide, *Phys. Rev. Lett.* 108 (2012) 246104.
- [16] S. Mammadov, J. Ristein, R.J. Koch, M. Ostler, Ch Raidel, M. Wanke, R. Vasiliauskas, R. Yakimova, Th Seyller, Polarization doping of graphene on silicon carbide, *2D Mater.* 1 (2014), 035003.
- [17] J. Stawińska, H. Aramberri, M.C. Munoz, J.I. Cerda, *Ab initio* study of the relationship between spontaneous polarization and p-type doping in quasi-free-standing graphene on H-passivated SiC surfaces, *Carbon* 93 (2015) 88–104.
- [18] P. Kaminski, R. Kozłowski, M. Miczuga, M. Pawłowski, M. Kozubal, J. Zelazko, „High-resolution photoinduced transient spectroscopy of defect centers in undoped semi-insulating 6H-SiC, *Mater. Res. Soc. Symp. Proc.* 1069 (2008), 1069-D02-01.
- [19] P. Kaminski, R. Kozłowski, M. Miczuga, M. Pawłowski, M. Kozubal, M. Pawłowski, „High-resolution photoinduced transient spectroscopy of defect centers in vanadium-doped semi-insulating SiC, *J. Mater. Sci. Mater. Electron.* (2008), <https://doi.org/10.1007/s10854-008-9576-6>.